3D Formation Flight using Differential Carrier-phase GPS Sensors [1]

Eric A. Olsen, Chan-Woo Park, Jonathan P. How
Stanford University

BIOGRAPHY

Eric Olsen is a Ph.D. candidate in the Dept. of Aeronautics and Astronautics at Stanford University. He received his BS in Aeronautics and Astronautics from the University of Illinois. His research involves the use of GPS for vehicle formation flying.

Chan-Woo Park is a Ph.D. candidate in the Dept. of Mechanical Engineering at Stanford University. He received his BS in Fiber and Polymer Science from Seoul National University. His research involves the use of GPS for autonomous spacecraft navigation.

Jonathan How is an Assistant Professor in the Dept. of Aeronautics and Astronautics at Stanford University. He received his B.A.Sc (1987) from the University. of Toronto, and SM (1990) and Ph.D. (1993) from MIT, both in the Dept. of Aeronautics and Astronautics.

ABSTRACT

This paper describes research on 3D formation flight using carrier-differential GPS sensors. Although absolute position at the centimeter level is generally not possible in real-time, relative position between vehicles within the formation can be obtained at these levels of accuracy using carrier phase differencing. However, several challenges exist before these measurements can be used in the formation state estimation, including solving for the integer biases. A method to generate a formation maneuver to rapidly solve for these biases is presented.

In order to better understand the problems associated with 3D formation flight, a new testbed has been developed. This testbed currently consists of two lighter-than-air vehicles (blimps) that operate in an indoor GPS laboratory. Operating indoors has several advantages, but also presents some significant challenges. A description of both the indoor environment, and the GPS receiver developed for this application is given. Finally, experimental results are presented for a single blimp performing a large scale autonomous flight and landing. Data is also presented for the two vehicle formation undergoing several maneuvers.

[1]Presented at the Institute of Navigation GPS Meeting, Nashville, TN, September 18, 1998.

1 INTRODUCTION

A revolution in spacecraft guidance, navigation and control technology has started through the use of GPS to autonomously provide vehicle position, attitude, and timing information. Not only will these innovations result in significant reductions in the weight, power consumption, and cost of future spacecraft attitude and orbit determination systems, they should also result in a significant reduction in ground operations costs through enhanced vehicle autonomy [1]. Recent results have demonstrated that Carrier-Phase Differential GPS (CDGPS) techniques can also be used to autonomously track and then control the relative position and attitude between several spacecraft [1, 2, 3, 4, 5, 6, 7, 8]. This sensing technology can be used to develop a *virtual spacecraft bus* using automatic control of a cluster of micro-satellites to replace the monolithic bus of current Earth Sciences Enterprise satellites (*e.g.* Landsat-7) [3, 6].

Many future space applications will benefit from using this formation flying technology to perform distributed observations, including enhanced synthetic apertures for earth mapping interferometry, and improved coverage for communication and surveillance. The goal of the overall research program is to demonstrate that we can accomplish these missions using a distributed array of very simple, but highly coordinated micro-satellites. This distributed approach provides many performance and operations advantages, including:

1. Extensive co-observing programs can be conducted autonomously without extensive ground support.
2. Increased baselines between instruments provides improved stellar interferometry. Use of many distributed micro-satellites improves world coverage.
3. Replacing traditional complex spacecraft with an array of simpler micro-satellites improves flexibility and offers a high degree of redundancy and reconfigurability in the event of a vehicle failure.
4. The low-cost, short lead-time instruments can be built, launched, and operated immediately. The expensive, long lead-time instruments can then join the fleet when available.

The concept of autonomous formation flying of satellite clusters has been identified as an enabling technology

for the success of various future missions of NASA and the U.S. Air Force. For example, the Earth Orbiter-1 (EO1) [1] and New Millennium Interferometer (NMI) [8], are two current NASA projects that seek to demonstrate the feasibility of multiple spacecraft formation flight. Similarly, the Air Force TechSat-21 [9] seeks to push the frontier in formation flying to enable global awareness and rapid access to space.

Implementation of the distributed coordinating satellite concept will require tight maintenance and control of the relative distances and phases between the participating satellites. Thus the benefits of this new approach come at a cost because the new systems architecture poses very stringent challenges in the areas of:

- Onboard sensing to perform the autonomous closed-loop relative navigation, attitude determination, and control.
- High-level mission management and planning to enable task allocation across the fleet of spacecraft.
- High-level fault detection recovery to enhance the mission robustness.

A ground-based command and control system for relative spacecraft positioning task would be very complex, heavily over-burdened, and may not provide sufficiently rapid corrective control commands. Thus, the onboard autonomy of the future spacecraft must be significantly enhanced to reduce the ground support required. The results discussed in this paper demonstrate that CDGPS sensing could play an important role in the guidance and control system needed to achieve the demanding relative navigation requirements of an on-orbit formation flying missions.

2 PREVIOUS WORK

Our work builds on previous research by Zimmerman that demonstrated the use of CDGPS for spacecraft rendezvous and capture between two simulated spacecraft in an indoor, 2D Laboratory GPS environment created by six pseudolites [2]. Several further studies of formation flying technologies [3] and experiments in GPS sensing for a three-vehicle formation [6] have also been performed in this Laboratory. These prior tests were limited to **2D** and **short baselines**. These constraints are physically restrictive, but there is a more significant problem with this configuration. In particular, the 2D testbed does not allow a complete analysis of all GPS errors that will be important for outdoor and/or space demonstrations of formation flying. This motivated the need to develop the three dimensional (3D) testbed described in this paper.

3 TESTBED DESCRIPTION

3.1 Lighter-Than-Air Vehicles

The lighter-than-air vehicles (blimps) used in this research are shown in Figure 1. The testbed currently consists

Fig. 1: Close-up shot of one of the blimps.

Fig. 2: Blimp gondola.

of two blimps that are controlled by standard RC motors. Each vehicle has a gondola that houses the motors, GPS receiver, radio modem, micro-controller, and batteries. The gondola carries five RC motors. Two motors provide vertical control,with a smaller motor being used for fine control when regulating altitude. The two motors at the ends of each gondola provide yaw control, and can also be used to move the blimp from side to side. The last motor provides thrust along the axis of the gondola for longitudinal control.

Blimp vehicles were selected because they are very easy to maintain and fly. Of course, the vehicles dynamics are quite different than would be expected for spacecraft on-orbit. But to create a formation of multiple vehicles, it is important to develop a simple design that is easily replicated. The key features of the blimps in Figure 1 are:

- 8 ft diameter by 14 ft long polyurethane bag and a balsa wood gondola (see Figure 2),
- 600 cubic feet of helium (net lift of 28.6 lbs),
- approximately 22 lbs of electronics and batteries,
- 3 GPS antennas and a modem communication link to the ground.

3.2 GPS Receiver

Figure 3 shows a picture of the GPS receiver that is on each blimp. The Mitel ORION^{TM} design is a single antenna receiver on a 3×4 inch printed circuit board. This design was modified to incorporate dual front ends on a single board, with a capability to use an off-board clock

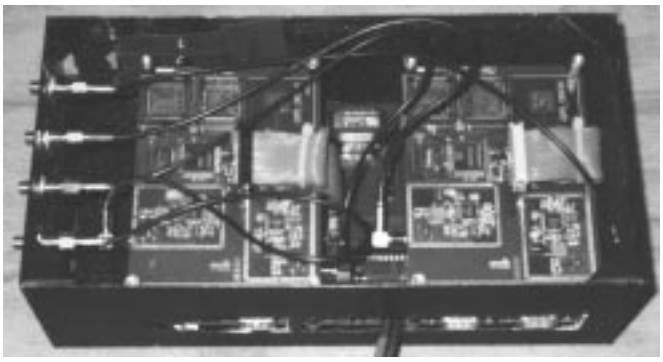

Fig. 3: The Mitel ORION Receiver

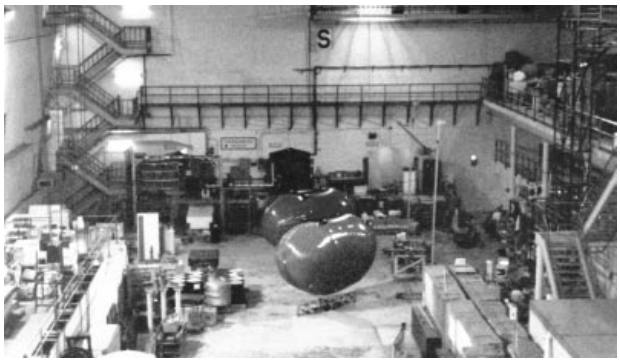

Fig. 4: Long range shot of the Highbay and blimps

signal to drive the receiver circuitry. These modifications allow for an arbitrary number of dual front-end receiver cards to be chained together using a common clock. In this configuration any number of antennas can be used to form a GPS based attitude system.

A key benefit of using the Mitel GPS hardware is that this also provides access to the GPS Builder Software (*GPS Architect* Toolkit). This software is almost entirely written in C code. Complete access to the code allowed us to extensively modify the code and carrier tracking loops, the signal acquisition algorithms, the cycle-slip detection routines, the input/output routines, and the frequency search region during startup.

The working receivers consist of two receiver cards mounted on a single interface board (Figure 3). This interface board provides power (including backup from a small NiCAD battery) to the receiver cards, a buffered clock signal to drive them, and three standard serial ports. There is a dedicated serial connection to each receiver card, and one serial port that is connected to both cards. This configuration enables information to be transmitted between the two cards (through their dedicated serial ports), while the interface to the entire receiver can be made through the joint serial port.

3.3 System Architecture

The current system architecture has the blimps communicating with a ground computer station that is used to perform the formation estimation and control calculations. These calculations will eventually be performed onboard and the vehicles will communicate to each other directly. Each vehicle transmits its GPS sensor measurements over the radio link to the ground station. The ground station updates the state estimates of the entire system, and then computes the necessary control commands to send to each vehicle. This greatly facilitates development since most of the code resides on the ground station where it can easily be debugged. Further, mission commands can be conveniently entered from the keyboard of the ground computer.

The system also has in place a fixed GPS reference station that allows operation of the system with only one vehicle. The reference station is optional when two or more vehicles are flying, but it can be used to simulate another vehicle within the constellation.

4 INDOOR GPS ENVIRONMENT ISSUES

4.1 Pseudolite Constellation

The longer term objective is to operate the vehicle formation outside so that we can use a combination of the NAVSTAR satellites and on-board pseudolites. However, the first testbed has been developed inside a large highbay at Stanford University. Figure 4 shows the highbay from the far end. The room used for the blimp tests has dimensions $200' \times 60' \times 60'$. Operations indoors offers several key advantages:

- Control over environment (no wind, rain),
- No need to move equipment (vehicles, computers) outside during development,
- Increased productivity.

However, the GPS signal is very weak, and is not available indoors. Thus, as with previous work on the 2D testbed [2, 3], we must build and maintain a *pseudo-constellation* of satellites.

The main issue when operating pseudolites indoors is a trade-off between effective workspace and multi-path. The GPS signal will reflect off the walls and other objects in the room. Multi-path will cause a small (several cm), but effectively random, error in the measurements as the formation maneuvers. Of more concern is the significant degradation in tracking performance that occurs because of the multi-path.

In an attempt to maximize the effective workspace, while at the same time keeping multi-path to a minimum, we investigated several antenna designs and experimented with the pseudolite placement. Previous solutions have used helical (directional) antennas. This minimizes multi-path since the signal is radiated over a small cone angle, but it introduces large gradients in the signal power over the workspace as a result of the natural antenna gain pattern. An alternative solution that was extensively tested is the use of patch antennas, which radiate with a near constant gain over most of a hemisphere. The radiating

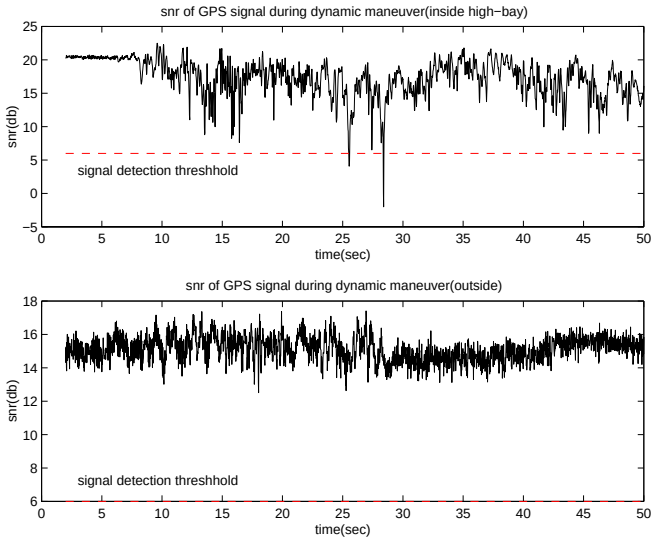

Fig. 5: SNR plot showing that the GPS signal suffers through momentary drops in power indoors. The signal power is much smoother outdoors.

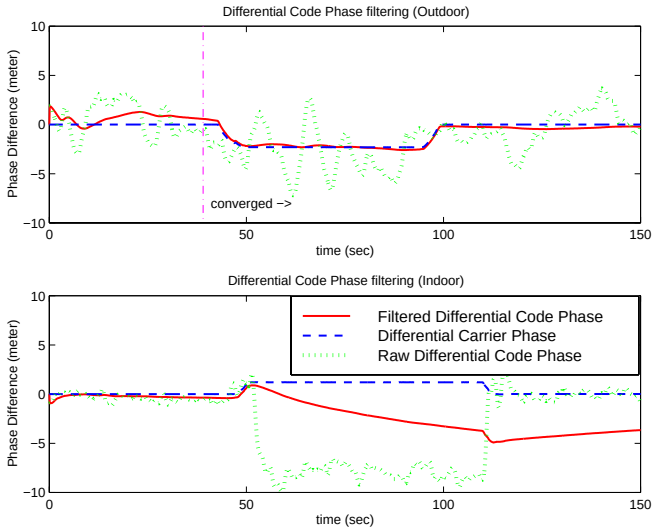

Fig. 6: Indoor and outdoor differential code (raw and smoothed). The plot shows that the high multi-path indoors could cause large positioning errors for measurements based on the smoothed differential code.

field can be choked to a desired cone angle by using an RF absorbent material tuned to the GPS frequency. This approach was tested in the highbay, but the experimental results indicated that there was excessive multi-path. This problem was further complicated by some apparent diffraction patterns near the edge of the cone angle.

The final *pseudo-constellation* consists of 8 pseudolites with helical antennas tuned to produce a radiating cone angle of about 50°. Two are located on the ceiling, above the workspace, while the other six are arrayed around the workspace, near the junction between the ceiling and walls. With this configuration, the effective GPS workspace is approximately $50' \times 25' \times 25'$.

4.2 Multi-Path

The most significant problem of working inside a building is the presence of multi-path signals from the reflections off the walls and other obstacles within the room. The subsequent interference pattern results in power nulls, and large power gradients within the workspace. Figure 5 shows a plot of the signal-to-noise ratio (SNR) for a received GPS signal as an antenna performs a dynamic maneuver. The results are shown for two separate maneuvers, one inside the highbay, and the other outside. The SNR inside the highbay shows significantly larger variations than the maneuver outside. Although the error in the carrier wave measurements are only a few centimeters, the highly localized power fluctuations can result in a complete loss of the signal, or cycle slips.

Both cases in Figure 5 used a software *integrate and dump* of 20 ms, corresponding to closing the tracking loops at 50 Hz. When the tracking loops are closed at 1 KHz indoors, the large SNR drops (which occur quite frequently, but over short time scales, *i.e.,* approximately a few ms) destabilize the loops. Performing a software integrate and dump over longer periods helps robustify the tracking loops to these problems. Further improvements in tracking performance are achieved using the knowledge of the instantaneous SNR value. When the SNR drops below some threshold (nominally the minimum GPS detection level), then the estimator should only perform the time update, and not perform the measurement update for that epoch. This allows the receiver to successfully "coast" through the brief signal drop outs associated with multi-path.

An experiment was also performed both indoors and outdoors to measure the relative effect of multi-path on code-phase measurements. In the experiment, differential phase data was collected while an antenna was moved around a fixed antenna for 2 minutes. As shown in Figure 6, the outdoor smoothed differential code phase change is coherent with the changes in the differential carrier phase. However, for the indoor case, the differential code and carrier phase changes are not coherent. Despite the fact that the SNR value for the indoor data was significantly higher than the SNR values for the outdoor data (a smaller variance in the raw code phase is noticeable in the indoor plot), the errors in the indoor smoothed differential code phase will degrade the positioning solutions. These results indicate that the carrier-smoothed differential code will be useful as an additional signal outside, but due to multi-path, will be of limited utility indoors.

5 FORMATION STATE ESTIMATION

5.1 Measurement Equations

This section provides the derivation of the equations used to estimate the relative position and attitude of the vehicles using the GPS carrier phase measurements. The

formulation here expresses the position of each vehicle in terms of absolute coordinates. Operations in space would use an approach based on a set of absolute coordinates for one vehicle, and a set of relative coordinates for each of the other vehicles within the formation.

The unknown state of the ith vehicle is the 7×1 vector $X_i = [P_i, \ E_i]$, where P_i is the position of vehicle i with coordinates (p_{ix}, p_{iy}, p_{iz}), and E_i is the orientation of the vehicle, represented in quaternion form $(\epsilon_{i1}, \epsilon_{i2}, \epsilon_{i3}, \epsilon_{i4})$.

The equations derived below assume that the phase measurements $\phi_{ijk}(t)$ are sampled at the same instant on all vehicles. This is not the case in reality, but the receiver can be modified so that the sample time is slewed at 1 Hz to a common time standard. This time standard is GPS time when the NAVSTAR constellation is visible, or the PRN code from an arbitrary pseudolite that is commonly visible to all vehicles when inside the highbay. This guarantees that all sample times are within approximately 100 ns of each other immediately after the slew. The error corresponding to this time offset is bounded by four times the maximum observed Doppler in the system times the maximum clock offset (100 ns) times the wavelength (0.19 m). Even for LEO, where the observed Doppler can be as large as 40 KHz, this error will be at the sub-centimeter level. A simple first order approximation to the phase rates can be used to account for any clock drift between the hardware slews of the sample time. Since the intra-vehicle differential phases are sampled simultaneously, this error shows up primarily in the relative positioning between vehicles.

The measured carrier phase at antenna j of vehicle i from transmitter k is given by

$$\phi_{ijk} = |S_{ijk}| + c\tau_{vi} + c\tau_{pk} + \lambda K_{ijk} \tag{1}$$

where S_{ijk} is a vector from the phase center of the pseudolite antenna to the phase center on each receive antenna, and K_{ijk} corresponds to the integer number of wavelengths. The terms $c\tau_{vi}$ and $c\tau_{pi}$ represent the portion of the phase incurred by clock errors between the transmitter and the receiver, and are the dominating terms in the measurement equations. These terms are eliminated by differencing over measurements from multiple antenna and vehicles. The antenna location relative to the transmitter is clearly a function of the vehicle position and attitude, so S_{ijk} is a function of the vehicle state X_i.

The intra-vehicle single differences contribute primarily to determination of the attitude of each vehicle. The attitude and position of each vehicle will be decoupled when using far transmitters only (*i.e.* NAVSTAR), but these vehicle states are coupled when near transmitters are used (*i.e.* transmitters on-board vehicles). These measurements are obtained by differencing between an arbitrarily designated master antenna ($j = m$) and the other antennas j of vehicle i for measurement from transmitter k:

$$\Delta\phi_{ijk} = |S_{imk}| - |S_{ijk}| + \lambda M_{ijk} \tag{2}$$

$\forall k$ and $\forall j \neq m$. The M_{ijk} in Eq. 2 are the intra-vehicle integers.

The inter-vehicle double differences contribute primarily to the determination of the relative positions between each vehicle. Given N transmitters, there are $N-1$ unique double differences between transmitters k_1 and k_2 ($k_1 \neq k_2$) for a pair of vehicles. These differences are calculated in order to eliminate the remaining effects due to clock differences between vehicles $c(\tau_{v1} - \tau_{v2})$

$$\begin{aligned} \nabla\Delta\phi_{ijk_1k_2} &= |S_{imk_1}| - |S_{jmk_1}| - (|S_{imk_2}| - |S_{jmk_2}|) \\ &+ \lambda N_{ijk_1k_2} \end{aligned} \tag{3}$$

$\forall k_1$, k_2 with $k_1 \neq k_2$. The $N_{ijk_1k_2}$ in Eq. 3 refers to the inter-vehicle integers.

All of these difference measurements are coupled to the states of the vehicles, so all of the measurements must be combined to obtain the entire formation state. From Eq 2, Eq 3, and the quaternion constraints, the complete set of measurements for a formation of n vehicles can be related to the vehicle states, and combined into an equation of the form:

$$y = h(x) + \beta + \nu \tag{4}$$

In this equation, y is the vector of measurements, $h(x)$ is the vector function of states, β is a vector of the inter and intra-vehicle biases, and ν is the measurement noise.

Given the phase measurements for the vehicle formation, the optimal estimate of the formation states $X_i(t)$ can be solved in real-time using nonlinear estimation techniques. However, as shown in Eq. 4 it is also necessary to obtain an estimate of the single and double difference integer ambiguities so that these can be subtracted from the phase measurements. This calculation solves for the absolute positions of the vehicles in the formation. The relative positions can then be found by differencing these absolute estimates. A CDGPS sensing system typically provides a much more accurate estimate of the relative position between the vehicles because many of the most important error sources are predominantly common-mode and their effects are removed by differencing the absolute position estimates.

An important effect that must also be accounted for in the measurement model results from the right hand circular polarization of the GPS signal. This is especially important in a spacecraft formation, wherein the vehicles can change their attitude and position relative to one another. See [10] for a complete description of this effect.

5.2 Formation Initialization

Before Eq. 4 can be used to solve for the state of the formation, it is first necessary to determine the biases.

These are usually determined by having the vehicle(s) undergo some motion relative to the transmitters and possibly each other. A batch least-squares or similar algorithm can then be employed to solve for the biases and states during the initialization maneuver. The spacecraft baseline constraints allow the intra-vehicle biases to be solved with a relatively small amount of motion. Additionally, small baselines could be employed to get a nearly instantaneous estimate of these biases if the LOS to some transmitters are known accurately (as would be the case with far transmitters). The inter-vehicle biases do not have any baseline constraints associated with them, and as such require more motion to determine. The inter-vehicle biases can be determined by putting the constellation through an arbitrary maneuver if the vehicles undergo sufficient motion relative to the transmitters. However, it is of interest to determine, in some sense, the best maneuver to perform.

Of course, even if the optimal maneuver where known, it typically could not be performed exactly because the formation does not have access to carrier-phase level state estimates until after the biases are determined. Additionally, the initial vehicle position uncertainties translate into errors in the optimization, especially if the vehicles have on-board transmitters. However, the formation can use code-differential phase to provide (≈ 2) meter-level position estimates during the initialization maneuver. By attempting to execute the optimal maneuver, the cluster should then be much better off than if it just performed random relative motions.

First consider a standard approach. An estimate of the biases can be formed by collecting measurements while the formation is in relative motion. Over N time epochs, this results in the set of equations

$$y_k = h_k(x_k) + \beta + \nu_k, \quad k = 1, \ldots, N \tag{5}$$

Eq. 5 can be linearized about the current best guess of $\hat{x}_k$ and $\hat{\beta}$ to give

$$y_k \cong h_k(\hat{x}_k) + H_k(\hat{x}_k)\delta x_k + \hat{\beta} + \delta\beta + \nu_k \tag{6}$$

and

$$\rho_k = y_k - h_k(\hat{x}_k) - \hat{\beta} \cong H_k(\hat{x}_k)\delta x_k + \delta\beta + \nu_k \tag{7}$$

Stacking these equations for all $k = 1, \ldots, N$ gives

$$\begin{aligned} \rho &= \begin{bmatrix} \rho_1 \\ \rho_2 \\ \vdots \\ \rho_N \end{bmatrix} = \begin{bmatrix} H_1 & & & 0 & I \\ & H_2 & & & I \\ & & \ddots & & \vdots \\ 0 & & & H_N & I \end{bmatrix} \begin{bmatrix} \delta x_1 \\ \delta x_2 \\ \vdots \\ \delta x_N \\ \delta\beta \end{bmatrix} + \nu \\ &= \tilde{H} \begin{bmatrix} \delta x \\ \delta\beta \end{bmatrix} + \nu \end{aligned} \tag{8}$$

where $H_k = H_k(\hat{x}_k)$. The weighted least squares solution is found by iterating on the solution of

$$\begin{bmatrix} \delta\hat{x} \\ \delta\hat{\beta} \end{bmatrix} = (\tilde{H}^T R^{-1} \tilde{H})^{-1} \tilde{H}^T R^{-1} \rho \tag{9}$$

where

$$\hat{x}_{\text{new}} = \hat{x}_{\text{old}} + \delta\hat{x} \tag{10}$$

$$\hat{\beta}_{\text{new}} = \hat{\beta}_{\text{old}} + \delta\hat{\beta} \tag{11}$$

Although the actual path that any vehicle takes will be continuous, data will only be collected at discrete intervals. As such, the approach taken here is to construct a quasi-optimal maneuver from a series of way-points. For simplicity, adjacent way-points are constrained to be equidistant from each other. Observability of the biases requires a geometry change in the transmitter/vehicle system. Data should be collected at points sufficiently far apart to insure that $\tilde{H}$ is full rank.

An important consideration when initializing the formation is the mean or maximum covariance of the biases that result from the estimation. The variance of any particular bias is the corresponding diagonal element of $(\tilde{H}^T\tilde{H})^{-1}$, where $\tilde{H}$ is evaluated at the estimate solution. Thus, to optimize a path to follow, we could use a cost function based on the bias covariances. The optimization in this case is formulated as

$$\min J = \textbf{trace}\ (P_b) \tag{12}$$

subject to

$$\|W_i^j - W_{i+1}^j\| = d_j \tag{13}$$

for $i = 1, \ldots, m-1$, and $j = 1, \ldots, s$, where

P_b = lower-right sub-matrix of $(\tilde{H}^T\tilde{H})^{-1}$ corresponding to the N_b biases,

m = number of way-points chosen,

s = number of vehicles,

W_i^j = ith way-point for the jth vehicle,

d_j = distance between way-points for vehicle j.

The solution to this problem provides a quasi-optimal path in which the covariance of the biases (in P_b) will be minimized for a given path length (as determined by m and d_j). Equivalently, the shortest path could be determined for a desired covariance level by iterating on either m, d_j, or both. The relative time history of each vehicle's motion is determined by the way-points.

This optimization problem cannot be solved analytically, and hence must be done numerically. A good initial estimate for the way-point history can be determined by maximizing the change in the Jacobian, H_k, from one

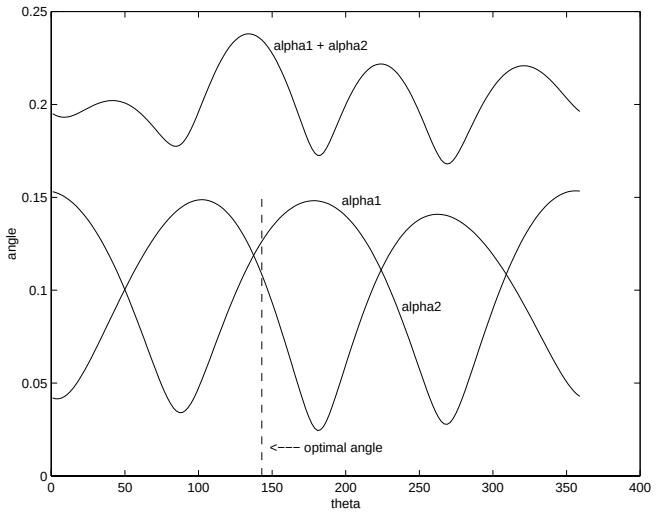

Fig. 7: Plot showing that the optimal starting trajectory is very near the point where the Jacobian experiences the largest change between the first two way-points

epoch to the next. To proceed, break out the columns of the Jacobian matrix

$$H_i = \left[\begin{array}{cccc} H_i^1 & H_i^2 & \dots & H_i^n \end{array} \right] \quad (14)$$

$$H_{i+1} = \left[\begin{array}{cccc} H_{i+1}^1 & H_{i+1}^2 & \dots & H_{i+1}^n \end{array} \right] \quad (15)$$

Then the angle, α, between any two columns is related to

$$\alpha_k = \arccos \frac{H_i^k \cdot H_{i+1}^k}{\|H_i^k\| \ \|H_{i+1}^k\|} \quad (16)$$

Hence, a measure of the change between the Jacobian matrices is $\sum_{i=1}^{n} \alpha_i$.

Figure 7 was generated for a 2D example with 6 transmitters arrayed in a near constellation. The optimal path was generated using 3 way-points for a single vehicle. The angles, α_1 and α_2 calculated from the Jacobians at the first and second way-points are shown, along with their sum. The angle between the two way-points (2D) is expressed by θ. The plot shows that although the overall trajectory is not at the angle θ which maximizes $\sum_{i=1}^{2} \alpha_i$, it is very close. This result is intuitive because the best path would maximize the observability of the biases. A series of way-points could be generated by this simplified methodology to provide a good initial guess for the optimization problem.

5.3 Bias Reacquisition

One or more biases will need to be recomputed when a GPS signal is lost and subsequently reacquired. For the indoor testbed described here, that occurs very frequently since most motions move the blimps into regions of the room wherein a particular signal is not visible. In the auto-landing described in section 6, that occured dozens of times. It is possible to bring back individual biases as long as an accurate estimate of the formation state is known. However, in doing so a completely consistent set of biases will not be obtained, and any formation state estimate error will creep into the bias estimate. A better solution is to continually update the bias estimates during operations. This is especially important in a high multi-path environment, since the biases can be corrupted by localized multi-path signals.

6 EXPERIMENTAL RESULTS

Several flight tests were conducted to demonstrate the performance of the integrated GPS system. These experiments were designed to exhibit key features of the GPS sensors and the algorithms required for formation-flying vehicles. This section presents two indoor flight tests:

1. Demonstration of an autonomous take off and landing of a single vehicle.
2. Demonstration of two vehicles performing autonomous maneuvers while maintaining formation.

6.1 Auto Landing Test

The automatic landing tests were developed as a comprehensive demonstration of the entire system, including the GPS sensors, and the estimation and control algorithms. These experimental results demonstrate the robust performance of the state estimation and control of a single vehicle, which is a key step towards formation flight.

At the start of the sequence the blimp was placed on a randomly located platform. A command to land on another randomly placed platform was then sent to the vehicle. The platform (dimensions 46" x 25") was placed at a known point, 4 ft from the ground level. The location of the landing site was provided to the blimp prior to take-off. The blimp took-off vertically from the first platform, and then set a heading towards the landing point. The blimp maintained a constant altitude and heading during most of the transit. A typical 3-D autonomous flight trajectory is shown in Figure 8.

Figure 9 shows the time history plot of the horizontal and vertical position estimates from the GPS sensor while performing an autonomous take-off and landing sequence. The altitude was set at 2.23 ft above the landing platform. Note that after approximately 50 seconds, when the horizontal position had settled, the blimp started the landing sequence by initiating a descent of 2 inches/sec while holding the horizontal position.

Figures 10 and 11 show the 10 horizontal landing points as measured on the table and estimated by GPS sensor, respectively. The negative bias in the Y direction appears to be a combined effect of a misalignment of the vertical direction thruster and low gain in Y-axis control. The measured and estimated landing points are summarized in Table 1. Note that the target landing point was X=-30.0 ft, and Y=0.0 ft in these experiments. The table shows that the estimated and measured landing points

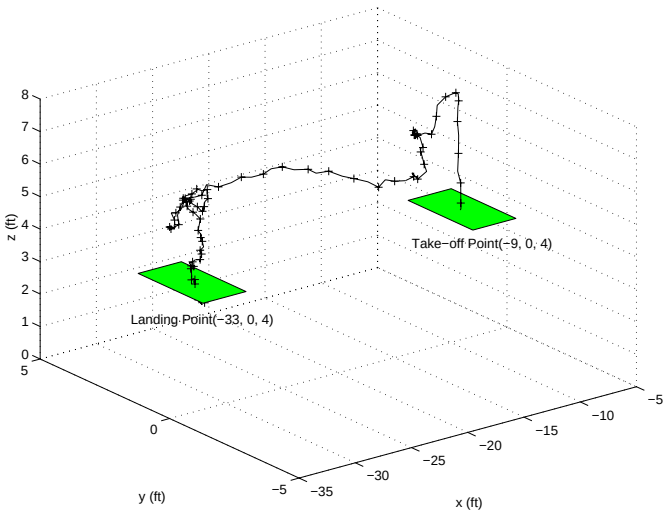

Fig. 8: 3-D Plot of Auto Landing Flight Path

Table 1: Results of 10 Auto Landing Results.

Horizontal Landing Point	X		Y		Distance from Target	
	Mean	STD	Mean	STD	Mean	STD
Measured (ft)	-30.06	0.21	-0.55	0.23	0.59	0.24
Estimated (ft)	-30.07	0.24	-0.71	0.20	0.76	0.19

are tightly clustered (standard deviation less than 0.24 ft for both).

No truth sensor is available to validate the state estimation during flight, so we can only test the accuracy of the GPS estimator at the landing point. The landing points were measured by a ruler once the blimp finished the descent sequence, and the accuracy of this manual measurement is on the order of 0.2 inches. Table 2 summarizes the estimation errors for the 10 autonomous landings. The errors are presented in terms of the inertial X and Y coordinates. We also give the horizontal distance between the estimated and measured landing points. The average value of the horizontal estimation error (distance error) was only 0.23 ft. Considering the HDOP value of 1.25 and multi-path effects in the testbed, horizontal errors of 0.23 ft can be expected based on carrier phase measurement noise levels. The VDOP in the testbed (5.03) is four times larger than the HDOP. This, combined with large multi-path error, can cause relatively large errors in the vertical position estimate. This error can be seen in Figure 8 and Figure 9, as demonstrated by the fact that the vertical position estimate was approximately 0.4 ft below the height of the actual landing platform (4 ft high) at the conclusion of the flight.

So, in spite of these problems (which are entirely consistent with the RF environment of the highbay) these results capture a very successful demonstration of precise vehicle estimation and control.

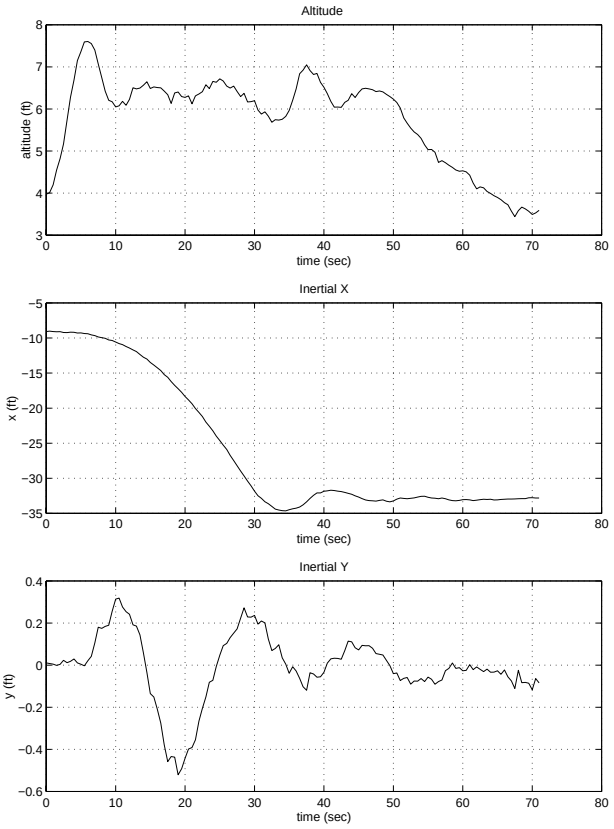

Fig. 9: Vertical and horizontal flight paths.

Table 2: Estimation Error in Landing Points.

Horizontal Estimation Error (ft)	X error		Y error		Distance error	
	Mean	STD	Mean	STD	Mean	STD
Estimate - Measurement	-0.01	0.14	-0.16	0.17	0.23	0.13

6.2 Formation Flight Test

A second experiment was performed with the two vehicles to demonstrate the complete 3D formation flying capability. The vehicles were arranged to fly in a line formation, and were initialized at random orientations and distances apart. The maneuvers for the formation were a complicated combination of changes in the horizontal position, altitude, and yaw angle. During these maneuvers, the controller attempted to maintained the initial relative X and Y distances between the two blimps while also maintaining an identical altitude and yaw angle. The follower vehicle (Blimp-1) reacted to changes in the lead vehicle's (Blimp-2) position and attitude.

In the results shown here, the blimps started 24 ft apart in X and 0 ft apart in Y. The altitudes were approximately 1 ft (0.3 m) apart. The heading angles were both 0°. The 3D position and orientation data was taken from the GPS sensors for 100 seconds. The leader vehicle was commanded to move about 3 ft forward and then 3 ft backward. Additionally, it was commanded to perform a full 180° yaw motion (two 90° steps) and undergo a

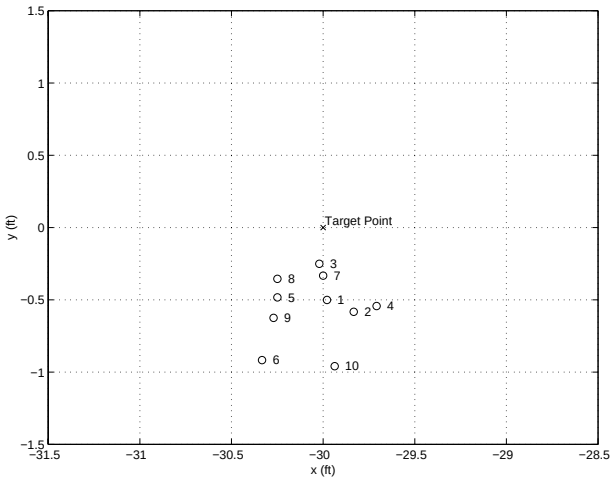

Fig. 10: Measured Landing Points

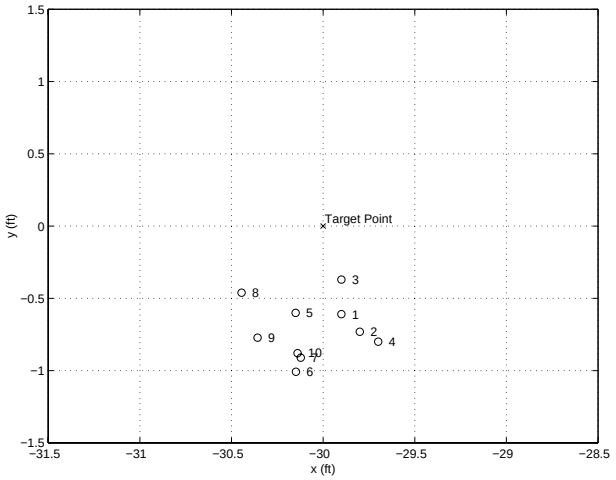

Fig. 11: Estimated Landing Points

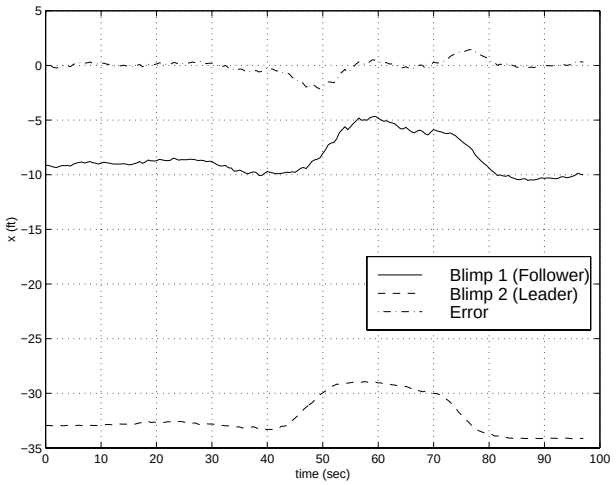

Fig. 12: X Axis Position of Formation Flying Blimps

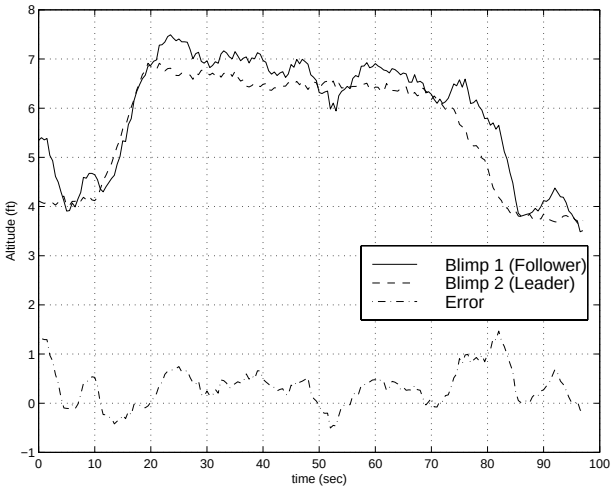

Fig. 13: Altitude of Formation Flying Blimps

change in vertical height.

Figures 12, 13 and 14 show the time histories for the X, Z, and Ψ states for the two vehicles. A time lag in the response of the follower vehicle (Blimp-1) is evident in the data. This lag is a result of the relative control architecture, and could be eliminated with a feedforward control scheme wherein the leader broadcasts the maneuvers to the follower vehicle as they are implemented.

The system errors are represented by the differences in the altitude, yaw angle , and the horizontal displacement (current blimp X and Y position minus the initial X and Y position) of the two vehicles. These errors are shown in Figures 12, 13 and 14.

7 CONCLUSIONS

This paper discusses 3D formation flight of several lighter-than-air vehicles in an indoor GPS laboratory. A method to generate a formation maneuver to rapidly solve for the integer biases was presented. The indoor GPS environment was described, along with the GPS receiver developed for this application. Experimental data for the first blimp formation test flights was also presented.

8 ACKNOWLEDGMENTS

This project is funded by Draper Laboratories under DL-H-505325 with Dr. Timothy Brand as the technical monitor.

References

[1] F. Bauer, J. Bristow, D. Folta, K. Hartman, D. Quinn, and J. P. How, "Satellite formation flying using an innovative autonomous control system (autocon) environment," in *AIAA/AAS Astrodynamics Specialists Conference*, (New Orleans, LA), Aug. 1997.

[2] K. R. Zimmerman and R. H. Cannon Jr., "Experimental demonstration of GPS for rendezvous between two prototype space vehicles," in *Proc. of the Institute of Navigation GPS-95 Conference*, (Palm Springs, CA), September 1995.

[3] J. C. Adams, A. Robertson, K. Zimmerman, and

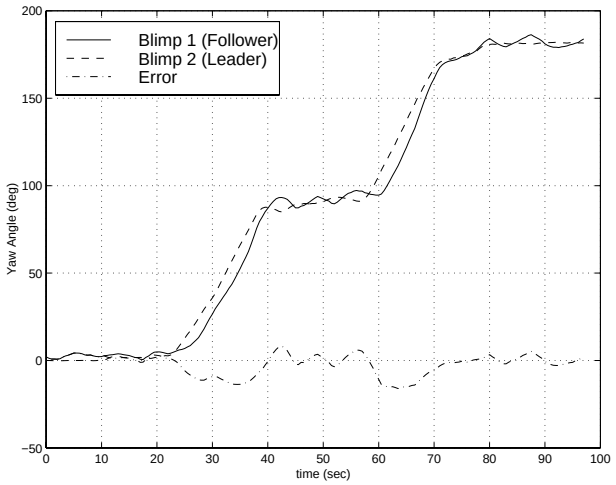

Fig. 14: Yaw Angle of Formation Flying Blimps

J. P. How, "Technologies for spacecraft formation flying," in *Proc. of the ION GPS-96 Conference*, (Kansas City, MO), Sept. 1996.

[4] D. Folta, L. Newman, and T. Gardner, "Foundations of formation flying for mission to planet earth and new millennium," in *AIAA/AAS Astrodynamics Specialists Conference*, July 1996.

[5] J. Guinn and R. Boain, "Spacecraft autonomous formation flying earth orbiters using GPS," in *AIAA/AAS Astrodynamics Specialists Conference*, July 1996.

[6] T. Corazzini, A. Robertson, J. C. Adams, A. Hassibi, and J. P. How, "GPS sensing for spacecraft formation flying," in *Proc. of the ION GPS-97 Conference*, (Kansas City, MO), Sept. 1997.

[7] P. W. Binning, *Absolute and Relative Satellite to Satellite Navigation using GPS*. Dept. of Aerospace engineering sciences, University of Colorado, April 1997.

[8] K. Lau, S. Lichten, and L. Young, "An innovative deep space application of GPS technology for formation flying spacecraft," in *Proc. of the AIAA GNC Conf*, (San Diego, CA), July 1996.

[9] Available at **http://www.vs.afrl.af.mil/VSD/TechSat21/**.

[10] J. C. Adams, E. Olsen, and J. P. How, "Experiments in GPS Attitude Determination for Spinning Spacecraft with Non-aligned Antenna Arrays," in *Proc. of the ION GPS-98 Conference*, (Nashville, TN), Sept. 1998.